Supporting Information

Functionalizing Titanium Disilicide Nanonets with Cobalt Oxide and Palladium for Stable Li Oxygen Battery Operations

Xiahui Yao, Qingmei Cheng, Jin Xie, Qi Dong, Dunwei Wang[*]

Department of Chemistry, Merkert Chemistry Center, Boston College, 2609 Beacon St., Chestnut Hill, Massachusetts 02467

[*] Corresponding e-mail: dunwei.wang@bc.edu

Table of Content of Supporting Information

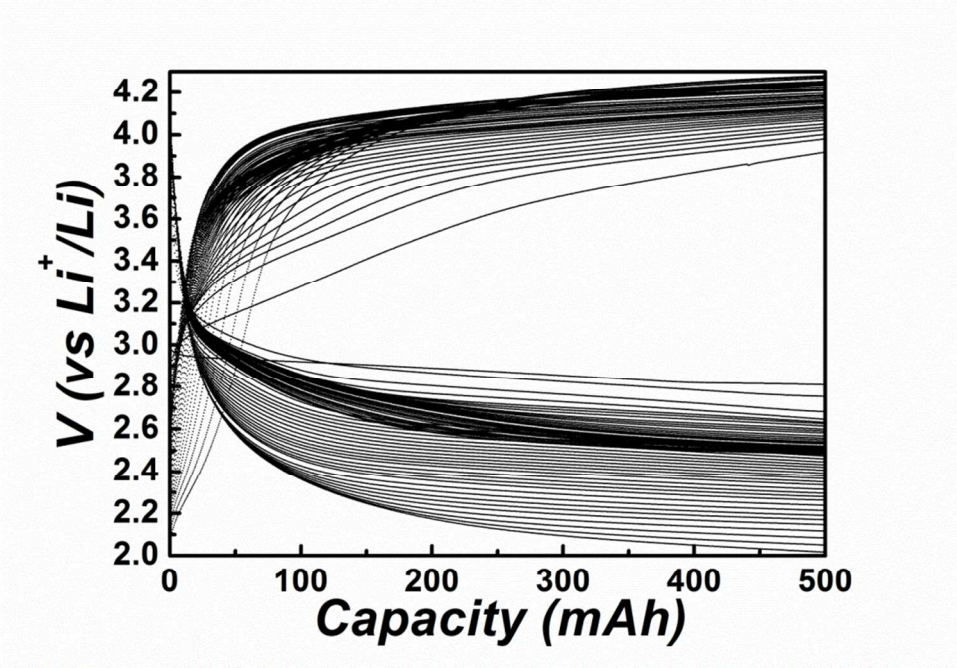

Figure S1. Voltage-capacity profile of $Pd/TiSi_2$, with $200mA/g_{Pd}$ current density for 63 cycles

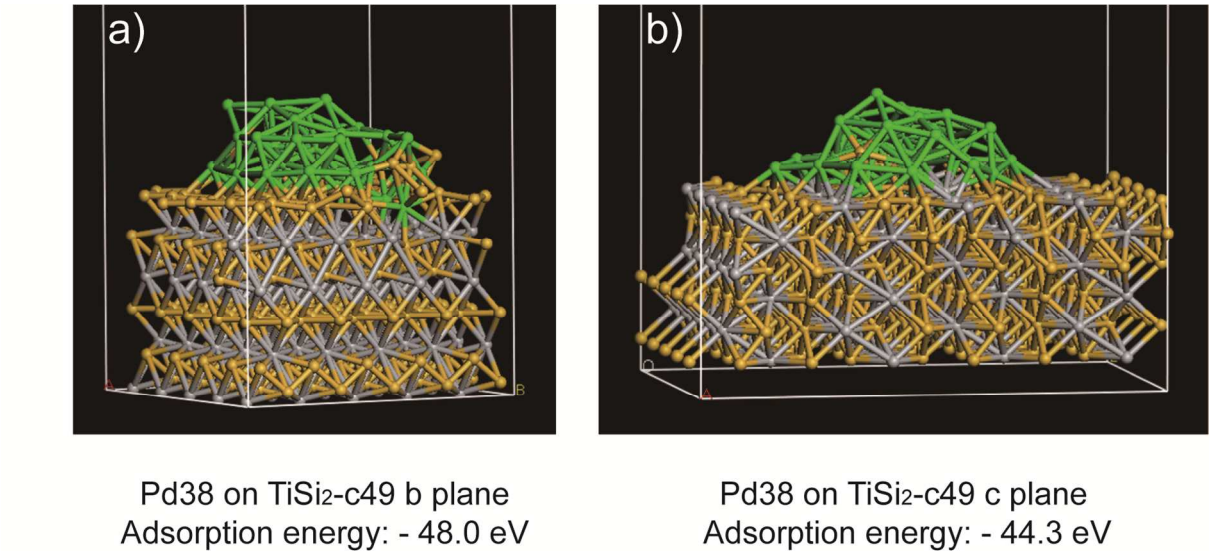

Figure S2. DFT calculation of the adsorption energy of a model Pd 38 cluster on different facets of $TiSi_2$. As a comparison, the adsorption energy for a Ru 38 cluster is -54.0 eV, and that for a Pt 38 cluster as -49.0 eV on the b plane of $TiSi_2$. (The majority of exposed surface of $TiSi_2$ nanonets is b plane.) Details of DFT calculation was reported previously.[1]

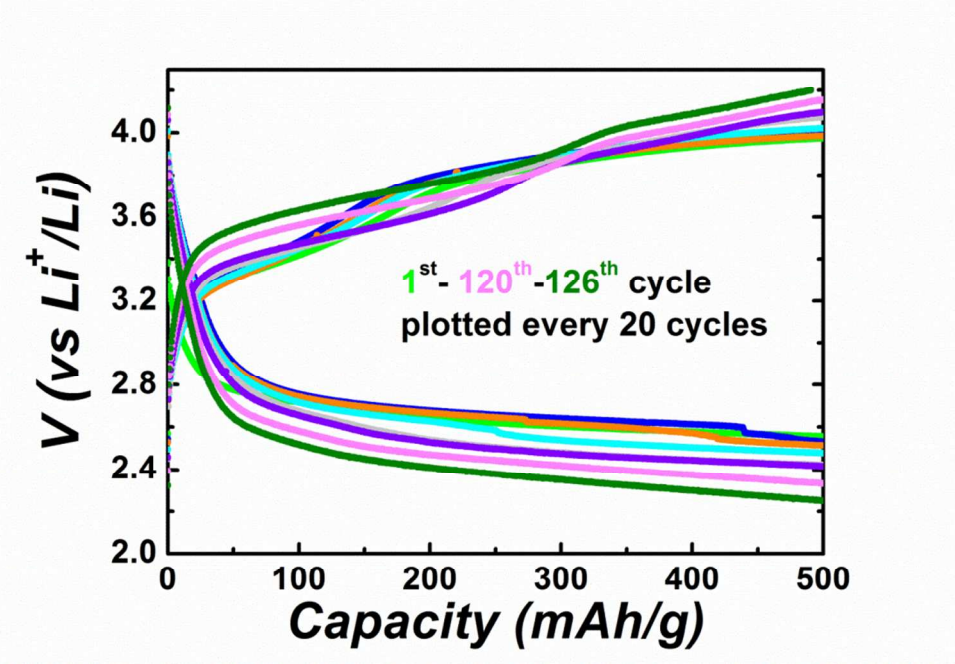

Figure S3. Voltage-capacity profile of $Pd/Co_3O_4/TiSi_2$ cathode for 126 cycles with 200 $mA/g_{Pd+Co3O4}$ current density

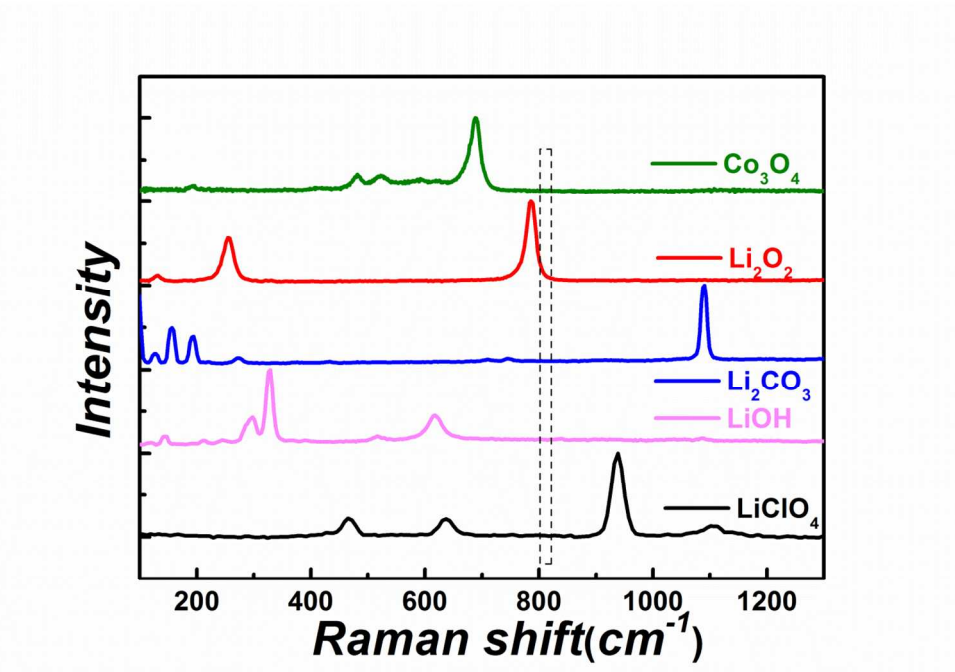

Figure S4. Raman spectra of potential chemical species.

Co_3O_4 was obtained by ALD on glass directly. Li_2O_2 (90% Sigma-Aldrich), Li_2CO_3 (99% Sigma-Aldrich), LiOH (98% Sigma-Aldrich) and $LiClO_4$ (99.99% Sigma-Aldrich) were from commercial powders.

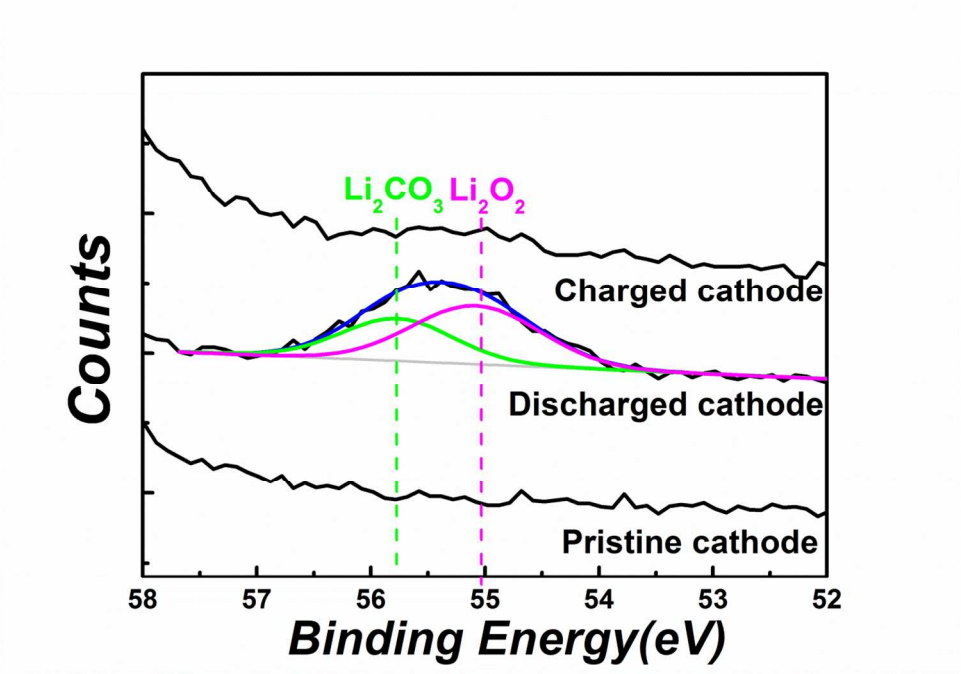

Figure S5. XPS of Li 1s spectra of pristine, discharged and charged Pd/Co_3O_4/$TiSi_2$ cathodes. The bump on the left (binding energy > 57 eV) was due to interference from Co 3p spectrum.

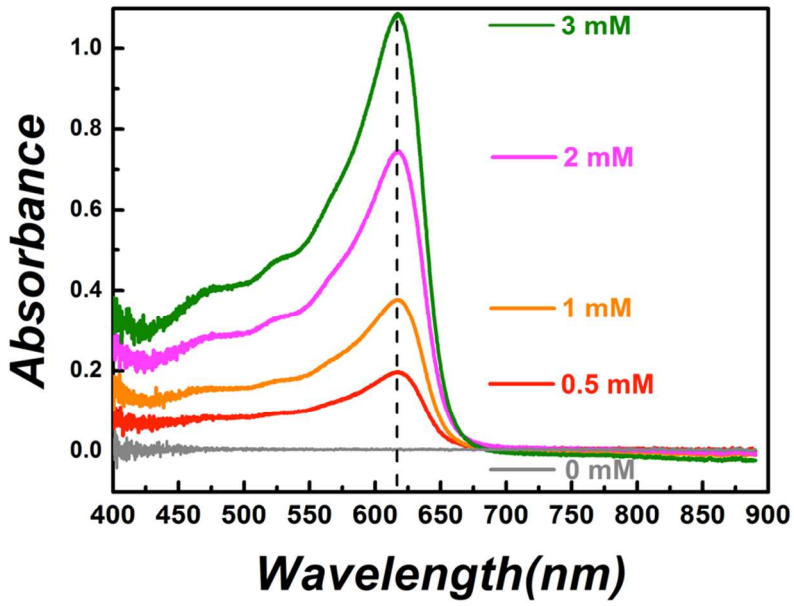

Figure S6. UV-Vis spectra of Fc^+ in DME with different concentrations

Table S1. Literature values of Li_2O_2 yields determination from electrochemical discharging

Method	Cathode and electrolyte	Yield	References
Iodometric	Vulcan or Super P carbon in DME	77~90%	[2]
Iodometric	Vulcan carbon in TEGDME	82%	[3]
Iodometric	Carbon nanotube in TEGDME	70%	[4]
TEMPO UV-Vis "back titration"	Carbon nanotube in DEME-NTf_2	>99%	[5]
Fc^+/Fc UV-Vis "back titration"	Vulcan Carbon in DME $Pd/Co_3O_4/TiSi_2$ in DME	74% 72.7~74.3%	Our result

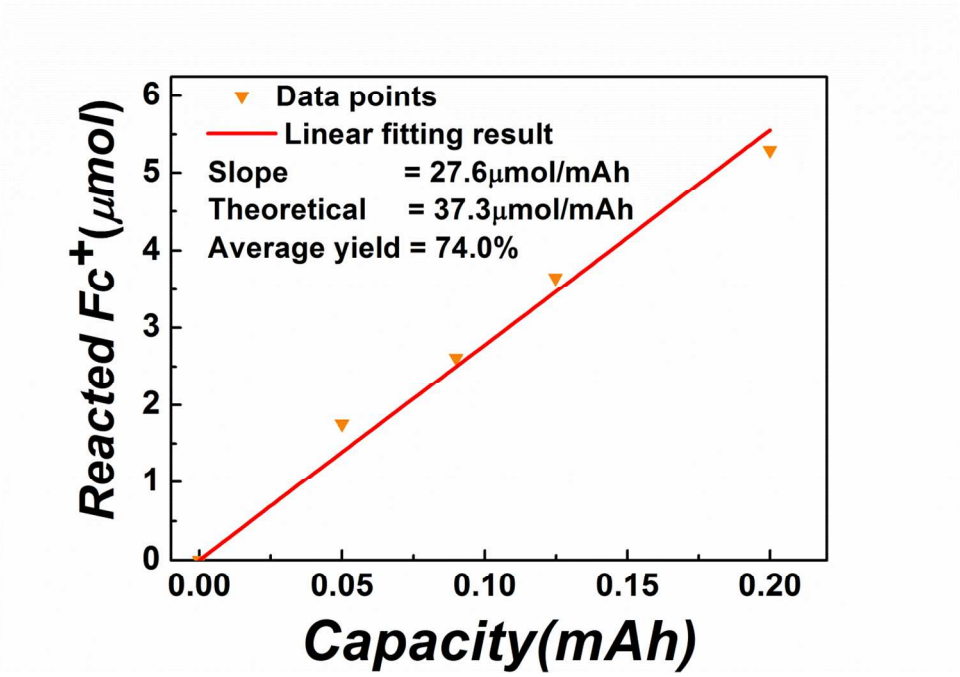

Figure S7. Quantification results of vulcan carbon cathodes

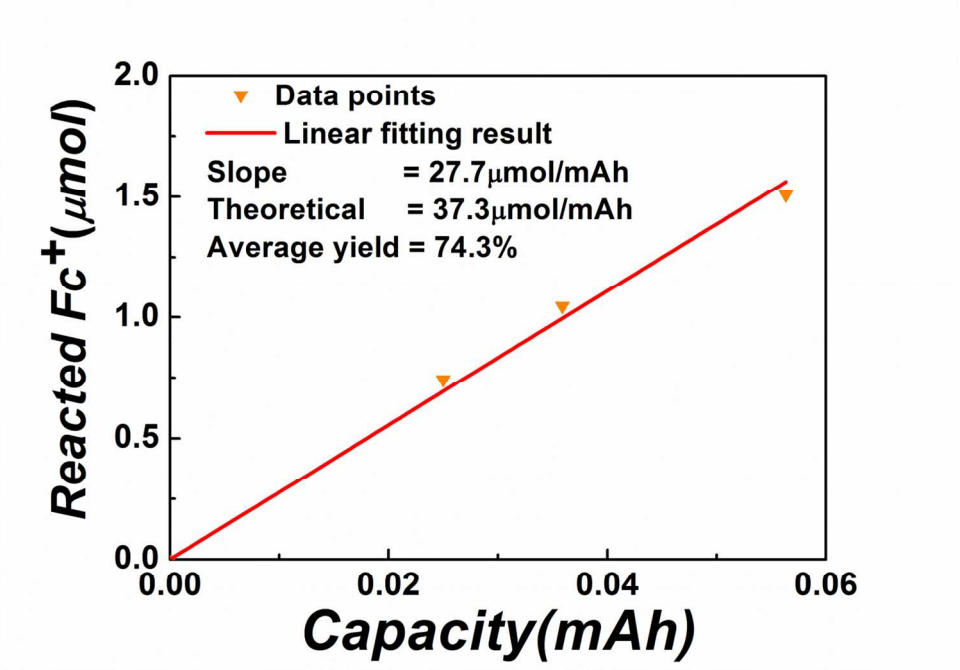

Figure S8. Li_2O_2 quantification results of discharged $Pd/Co_3O_4/TiSi_2$ cathode with 2.5V cut off voltage

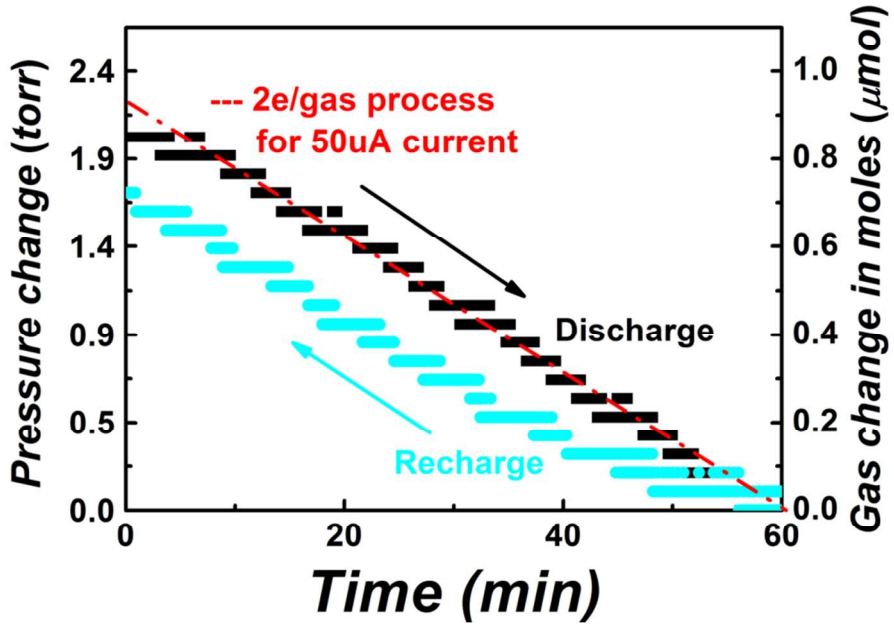

Figure S9. Gas consumption and generation of $Pd/Co_3O_4/TiSi_2$ cathode calculated from the pressure change of the cell head space during the discharge and recharge process. (Electrolyte: 0.1 M $LiClO_4$ in DME; Current: 50 μA; Head space volume: 8 mL; Temperature: 29 ^oC; Pressure sensor: MKS 902B, ±0.1 torr)

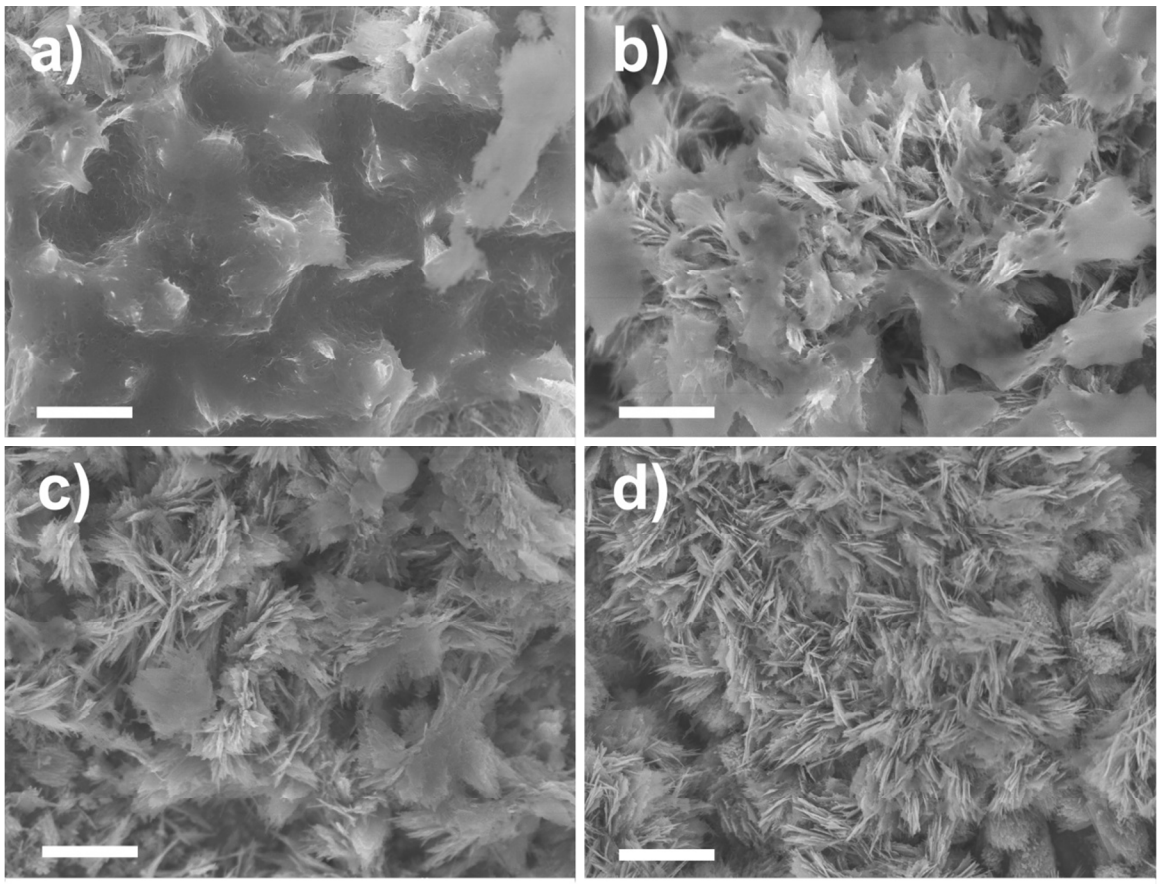

Figure S10. Morphology evolution of cathode surface at different stage during recharge: a) 0%, b) 50%, c) 90%, d) 100% recharged. All scale bars are 2μm.

The discharge product formed filled the space between the strands of the nanonets as can be observed in Figure S10a. During recharge, films are gradually removed to reveal the surface of the cathode (Figure S10b-d).

Unlike carbon on which the Li_2O_2 formed as toroid particle on top of the carbon surface, physically increasing the recharge over potential, nanonets structures or similar nanowire structures enabled the facile electron transport pathway by penetrating into the Li_2O_2 films (or particles) to facilitate the decomposition.

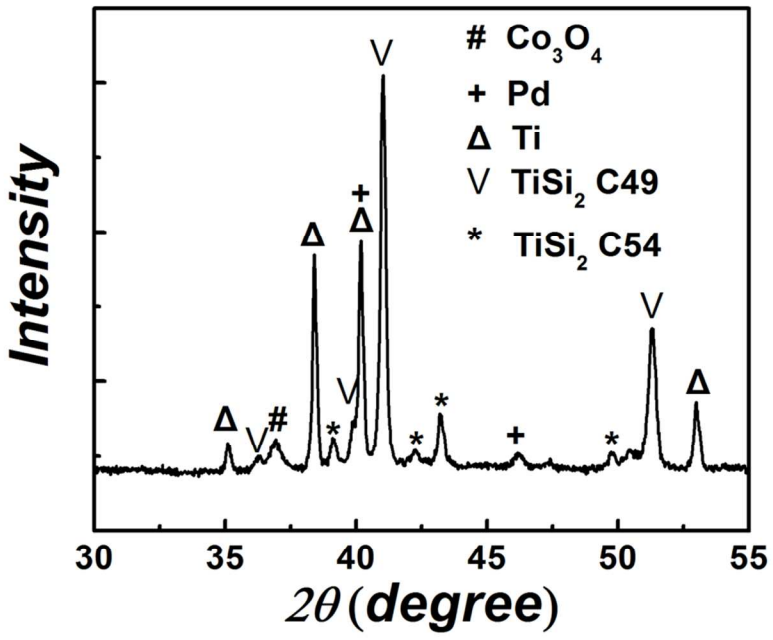

Figure S11. X-ray diffraction patterns of as-grown Pd/Co_3O_4/$TiSi_2$ on Ti mesh. Reference JCPDFS numbers are as follows, Pd: 05-0681; Co_3O_4: 042-1467; Ti: 05-0682; $TiSi_2$ C54: 02-1120; $TiSi_2$ C49: 10-0225. To be noted that the $TiSi_2$ nanonets have a slight shift comparing with standard C49 phase as indicated previously.[6]

References

(1) Xie, J.; Yao, X.; Madden, I. P.; Jiang, D.-E.; Chou, L.-Y.; Tsung, C.-K.; Wang, D. Selective Deposition of Ru Nanoparticles on $TiSi_2$ Nanonet and Its Utilization for Li_2O_2 Formation and Decomposition. *J. Am. Chem. Soc.* **2014**, *136*, 8903-8906.

(2) McCloskey, B. D.; Valery, A.; Luntz, A. C.; Gowda, S. R.; Wallraff, G. M.; Garcia, J. M.; Mori, T.; Krupp, L. E. Combining Accurate O_2 and Li_2O_2 Assays to Separate Discharge and Charge Stability Limitations in Nonaqueous Li-O_2 Batteries. *J. Phys. Chem. Lett.* **2013**, *4*, 2989-2993.

(3) Adams, B. D.; Black, R.; Radtke, C.; Williams, Z.; Mehdi, B. L.; Browning, N. D.; Nazar, L. F. The Importance of Nanometric Passivating Films on Cathodes for Li-Air Batteries. *ACS Nano* **2014**, *8*, 12483-12493.

(4) Nasybulin, E. N.; Xu, W.; Mehdi, B. L.; Thomsen, E.; Engelhard, M. H.; Massé, R. C.; Bhattacharya, P.; Gu, M.; Bennett, W.; Nie, Z.; Wang, C.; Browning, N. D.; Zhang, J.-G. Formation of Interfacial Layer and Long-Term Cyclability of Li-O_2 Batteries. *ACS Appl. Mater. Interfaces* **2014**, *6*, 14141-14151.

(5) Hase, Y.; Ito, E.; Shiga, T.; Mizuno, F.; Nishikoori, H.; Iba, H.; Takechi, K. Quantitation of Li_2O_2 stored in Li-O_2 Batteries Based on Its Reaction with an Oxoammonium Salt. *Chem. Commun.* **2013**, *49*, 8389-8391.

(6) Zhou, S.; Liu, X.; Lin, Y.; Wang, D. Rational Synthesis and Structural Characterizations of Complex $TiSi_2$ Nanostructures. *Chem. Mater.* **2009**, *21*, 1023-1027.